

NEW SHELL STRUCTURE ORIGINATED FROM THE COMBINATION OF QUADRUPOLE AND OCTUPOLE DEFORMATIONS[†]

K. ARITA[‡]

Department of Physics, Kyoto University, Kyoto 606-01, Japan

preprint KUNS1273, July 1994

Abstract

Semiclassical analysis of the shell structure for a reflection-asymmetric deformed oscillator potential with irrational frequency ratio $\omega_{\perp}/\omega_z = \sqrt{3}$ is presented. Strong shell effects associated with bifurcations of short periodic orbits are found, which occur for a combination of quadrupole and octupole deformations.

[†]Submitted to Physics Letters B.

[‡]E-mail: arita@ruby.scphys.kyoto-u.ac.jp

Study of reflection-asymmetric deformation is one of the exciting current subjects in both nuclear structure and micro-cluster physics [1–4]. As is well known, nuclear deformation is intimately related with the single-particle level structure. The system favors such shapes that exhibit strong shell effects and make the level density at the Fermi surface lower. We have analyzed in Refs. [5–7] shell structures in a superdeformed (SD) oscillator potential with the octupole deformation added. The model Hamiltonian adopted is

$$H = \frac{\mathbf{p}^2}{2M} + \sum_i \frac{M\omega_i^2 x_i^2}{2} - \lambda_{30} M\omega_0^2 [r^2 Y_{30}(\Omega)]'', \quad (1)$$

where the double primes denote that the variables in the square bracket are defined in terms of the doubly-stretched coordinate $x_i'' \equiv (\omega_i/\omega_0)x_i$. The frequency ratio ω_\perp/ω_z is taken to be 2 with $\omega_x = \omega_y = \omega_\perp$. At $\lambda_{30} = 0$, the shell structure for this Hamiltonian is mainly determined by the figure-8 type family of periodic orbits. However, the planar orbit family in the x - y plane having shorter period give rise to an interference effect on the shell oscillations and result in modulation pattern in the smoothed level density, called *supershell*. We found that the supershell effect significantly develops at octupole deformation parameter $\lambda_{30} \simeq 0.4$ [5]. This is explained as due to the changes in stabilities of the two classes of periodic orbits against the octupole deformation [6, 7].

As a continuation of the above work, we have carried out semiclassical analysis of the shell structure for the Hamiltonian (1) varying both λ_{30} and the axis ratio ω_\perp/ω_z . The details will be reported elsewhere [8]. As an illustrative example, we discuss here the case of an irrational axis ratio $\omega_\perp/\omega_z = \sqrt{3}$. Figure 1 shows the single-particle spectrum calculated as a function of λ_{30} . There is no prominent shell structure at $\lambda_{30} = 0$ because of irrationality of the frequency ratio. However, a significant shell structure appears at $\lambda_{30} \simeq 0.3$. The oscillating level density smoothed by the Strutinsky method is shown in Fig. 2. One clearly sees a prominent shell oscillation. Evidently, this shell structure arises as a consequence of the combination of quadrupole and octupole deformations. One may also notice a supershell structure, which is found to be associated with the interference between classical periodic orbits with the periods $T \simeq 2\pi/\omega_\perp$ and $2\pi/\omega_z$.

In classical mechanics, there are only two types of periodic orbits at $\lambda_{30} = 0$; one is the Isolated Linear orbit along the z -axis (IL) and the other is the continuous family of elliptic orbits in the x - y plane. Among the latter family, only the Planar-A type (PA) orbits (in the plane containing the symmetry axis) and an isolated circular orbit survive when the

octupole deformation is added. In Fig. 3, we show some short periodic orbits for $\lambda_{30} = 0.3$. It is noteworthy that orbit PB appears at $\lambda_{30} \simeq 0.29$ due to an isochronous bifurcation of orbit IL. Likewise, orbits PC and PD are born by a saddle-node bifurcation at $\lambda_{30} \simeq 0.28$. Orbits PE and PF arise from a period-tripling bifurcation of orbit PA at $\lambda_{30} \simeq 0.2$. To show how these bifurcations occur, we plot in Fig. 4 traces of the monodromy matrices [9] for these orbits as functions of λ_{30} . The monodromy matrix M describing linearized dynamics about the periodic orbit is defined by

$$M_r(Z_{r_0}) = \left. \frac{\partial Z_r^\perp(t = T_r)}{\partial Z_r^\perp(t = 0)} \right|_{Z_{r_0}}, \quad (2)$$

where Z denotes the phase space vector (\mathbf{p}, \mathbf{q}) , Z_{r_0} a point on the periodic orbit r , and T_r the period of the orbit. $Z^\perp(t)$ represents the components orthogonal to a manifold formed by the continuous set of the periodic orbit, and here has dimension 2 (or 4 for an isolated orbit). The eigenvalues of M are independent of Z_{r_0} and, due to the symplectic property, they are represented as $(+/-)(e^\alpha, e^{-\alpha})$, α being real or pure imaginary. Stable orbits have imaginary α and $|\text{Tr } M| < 2$, while unstable orbits have real α and $|\text{Tr } M| > 2$. The periodic orbit bifurcation occurs when the eigenvalues of M become unity, namely, when $\text{Tr } M = 2$. The bifurcations mentioned above are clearly seen in Fig. 4.

In order to see the feature of the bifurcations in detail, let us examine the Poincaré surfaces of section. Since the system under consideration has axial symmetry, it reduces to a two-dimensional system with cylindrical coordinates (ρ, z) having a fixed angular momentum p_φ . Figure 5 shows the Poincaré surfaces of section (ρ, p_ρ) defined by $z = 0$ and $p_z < 0$, for $p_\varphi = 0$. The orbit IL (corresponding to the origin) is stable at $\lambda_{30} = 0.28$ and accompanies tori about it. These tori are significantly distorted until a saddle-node bifurcation occurs at $\lambda_{30} \simeq 0.283$. In the figure for $\lambda_{30} = 0.29$ we thus find a new phase-space structure that accommodates two emergent periodic orbits; the stable orbit PD (corresponding to the pair of islands) and the unstable orbit PC (the pair of saddles). At $\lambda_{30} \simeq 0.292$, an isochronous bifurcation of orbit IL occurs, generating the stable orbit PB (corresponding to the new pair of islands seen in the figure for $\lambda_{30} = 0.3$), and the central torus becomes unstable.

Now let us recall the correspondence between quantum and classical mechanics. In the Gutzwiller trace formula, the density of levels $g(E) = \sum_n \delta(E - E_n)$ is represented as a

sum of contributions from classical periodic orbits [10]

$$g(E) = \bar{g}(E) + \sum_{nr} A_{nr}(E) \cos\left(\frac{nS_r(E)}{\hbar} - \frac{\pi}{2}\mu_{nr}\right). \quad (3)$$

The first term on the right-hand side is the Weyl term which is a smooth function of energy. The second term is composed of the periodic orbit sum (r denote each primitive periodic orbit and $n(\neq 0)$ the number of repetition of the orbit) and represents the quantum correction to the first term. $S_r = \oint_r \mathbf{p} \cdot d\mathbf{q}$ is the action integral along the orbit, and μ_{nr} denotes the Maslov phase. Our aim here is to analyze gross features of the single-particle spectrum, namely, the shell structure. Let δE denotes the energy resolution which we are interested in. Then the periods $T = \partial S / \partial E$ of contributing periodic orbits are restricted by the following relation:

$$\Delta S = S(E + \delta E) - S(E) \simeq T \cdot \delta E < 2\pi\hbar, \quad (4)$$

namely, by

$$T < \frac{2\pi\hbar}{\delta E}. \quad (5)$$

Thus, we need only to pick up these finite number of short periodic orbits. Next, let us discuss the amplitude factor $A_r(E)$ in the trace formula. For systems in which chaos is fully developed, periodic orbits show strong instability and are well isolated in the phase space, so that the stationary phase approximation (SPA) seems to work well. Then the trace integral can be performed by the SPA with the result

$$A_{nr}(E) = \frac{1}{\pi\hbar} \frac{T_r}{\sqrt{|\det(\mathbf{1} - M_r^n)|}}, \quad (6)$$

where M_r denotes the monodromy matrix and T_r the period of the primitive orbit r . This expression may be good when all eigenvalues of M_r^n are sufficiently far from unity. At the point where a pair of the eigenvalues becomes 1 (a bifurcation point of the orbit), this amplitude factor suffers divergence. It is due to the break down of the SPA: In the coordinate expansion about the stationary point, one of the coefficients of the quadratic terms vanishes and higher order nonlinear terms become important. Such a situation occurs quite often in mixed systems, where one observe admixture of regularity and chaos. This is an unsolved difficult problem of *quantizing soft chaos*.

To find the link between the quantum shell structure seen in Figs. 1, 2 and the properties of the periodic orbits, let us consider the Fourier transform of the single-particle level density [7]

$$F(s) = \int_0^\infty dE \frac{e^{isE}}{\sqrt{E}} g(E). \quad (7)$$

To remove the ambiguity associated with the cutoff in energy, we adopt a gaussian convolution with $f(x) = \exp(-x^2/2)$ as

$$F_{\Delta s}(s) = \int ds' f((s - s')/\Delta s) F(s'). \quad (8)$$

Using the scaling property of the system under consideration, $H(\alpha\mathbf{p}, \alpha\mathbf{q}) = \alpha^2 H(\mathbf{p}, \mathbf{q})$, the quantum and the semiclassical expressions for $F_{\Delta s}(s)$ become

$$F_{\Delta s}^{(\text{qm})}(s) = \sum_n \frac{e^{isE_n}}{\sqrt{E_n}} f(E_n/E_{\text{max}}), \quad (9)$$

$$F_{\Delta s}^{(\text{cl})}(s) = \bar{F}_{\Delta s}(s) + \sum_{nr} A_{nr}(1) e^{i\pi\mu_{nr}/2} f((s - nT_r)/\Delta s), \quad (10)$$

where the cutoff energy is defined by $E_{\text{max}} \equiv \hbar/\Delta s$. The semiclassical $F^{(\text{cl})}(s)$ has the functional form with successive peaks at the periods of classical periodic orbits, and the height of each peak represents the intensity of the corresponding orbit. Thus, one can extract information about classical mechanics by calculating the quantity (9) and comparing it with the expression (10). One may expect that the singularities in the classical phase space due to the periodic orbit bifurcations will affect the properties of the quantum system in a critical manner.

Figure 6 shows absolute values of the Fourier transform (9) as a function of both s and λ_{30} . It is seen that the peak at $s \simeq \sqrt{3}$ (in unit of $T_\perp = 2\pi/\omega_\perp$) significantly grows up as λ_{30} increases and reaches the maximum at $\lambda_{30} = 0.34$. At small λ_{30} , this peak is determined by the linearized dynamics about the orbit IL. As λ_{30} increases and approaches the bifurcation point $\lambda_{30} \simeq 0.3$, the peak becomes higher as expected from Eq. (6). In addition, the resonant torus (which brings about orbits PC and PD) also contributes to this peak because of the similarity of the frequencies. Furthermore, three-dimensional periodic orbits (having periods similar to them, not shown in Fig. 3) contribute to it too. Thus these bifurcations of orbits that take places at almost the same value of λ_{30} are responsible for the strong enhancement of the Fourier peak.

One should also note that the peak at $s \simeq \sqrt{3}$ takes the maximum, delaying somewhat from the bifurcation points $\lambda_{30} = 0.28 \sim 0.3$. Another peak at $s \simeq 3$, corresponding to orbit 3PA (triple traversals of orbit PA), reaches the maximum at $\lambda_{30} \simeq 0.28$, also showing a delay from the period-tripling bifurcation point $\lambda_{30} \simeq 0.2$ of orbit PA. Similar delay phenomena were noticed in our previous analysis for the SD case with the frequency ratio $\omega_{\perp}/\omega_z = 2$ [7]. Thus, we have found a presumably general tendency of the Fourier amplitude near bifurcations: The amplitudes exhibits significant enhancements due to the periodic orbit bifurcations, with the maximum point being somewhat shifted into the postbifurcation region. It would be very interesting to investigate these behaviors of the Fourier amplitudes in more detail.

In conclusion, we have made a semiclassical analysis of the shell structure for a reflection-asymmetric deformed oscillator. Prominent shell effects arise for a combination of the quadrupole and the octupole deformations. It is shown that these shell structure can be understood in terms of short periodic orbits and their bifurcations. It would be an interesting future subject to investigate how the new shell structure discussed in this paper persists in other reflection-asymmetric deformed potentials having radial dependence different from the oscillator-type. The author thanks Professor Matsuyanagi for many valuable discussions and carefully reading the manuscript.

References

- [1] S. Åberg, H. Flocard and W. Nazarewicz, *Ann. Rev. Nucl. Part. Sci.* 40 (1990) 439.
- [2] I. Hamamoto, B. R. Mottelson, H. Xie and X. Z. Zhang, *Z. Phys.* D21 (1991) 163.
- [3] W. D. Heiss, R. G. Nazmitdinov and S. Radu, *Phys. Rev. Lett.* 72 (1994) 2351.
- [4] S. Frauendorf and V. V. Pashkevich, *Rosendorf preprint FZR-37* (1994).
- [5] K. Arita and K. Matsuyanagi, *Prog. Theor. Phys.* 89 (1992) 389.
- [6] K. Arita, *Prog. Theor. Phys.* 90 (1993) 747.
- [7] K. Arita and K. Matsuyanagi, *Prog. Theor. Phys.* 91 (1994) 723.
- [8] K. Arita and K. Matsuyanagi, in preparation.
- [9] M. A. M. de Aguiar, C. P. Malta, M. Baranger and K. T. R. Davies, *Ann. Phys.* (N. Y.) 180 (1987) 167.
- [10] M. C. Gutzwiller, *J. Math. Phys.* 8 (1967) 1979; 12 (1971) 343.

Figure 1: Single-particle spectrum of the Hamiltonian (1) with the frequency ratio $\omega_{\perp}/\omega_z = \sqrt{3}$, plotted as a function of λ_{30} . Dashed and solid lines represent levels with zero and nonzero K -quantum numbers, respectively. Each solid line is composed of two degenerate levels with K and $-K$. Magic numbers appearing at $\lambda_{30} \approx 0.3$ are indicated taking the spin degeneracy factor 2 into account.

Figure 2: Oscillating level density $g_{\text{osc}}(E) = g(E) - \bar{g}(E)$ for $\lambda_{30} = 0.3$. The Strutinsky energy smoothing is done to a width $\delta E = \hbar\omega_{\perp}/2$. The numerals indicate the magic numbers corresponding to the shell gaps.

Figure 3: Some classical periodic orbits for the Hamiltonian (1) with the frequency ratio $\omega_{\perp}/\omega_z = \sqrt{3}$ and $\lambda_{30} = 0.3$.

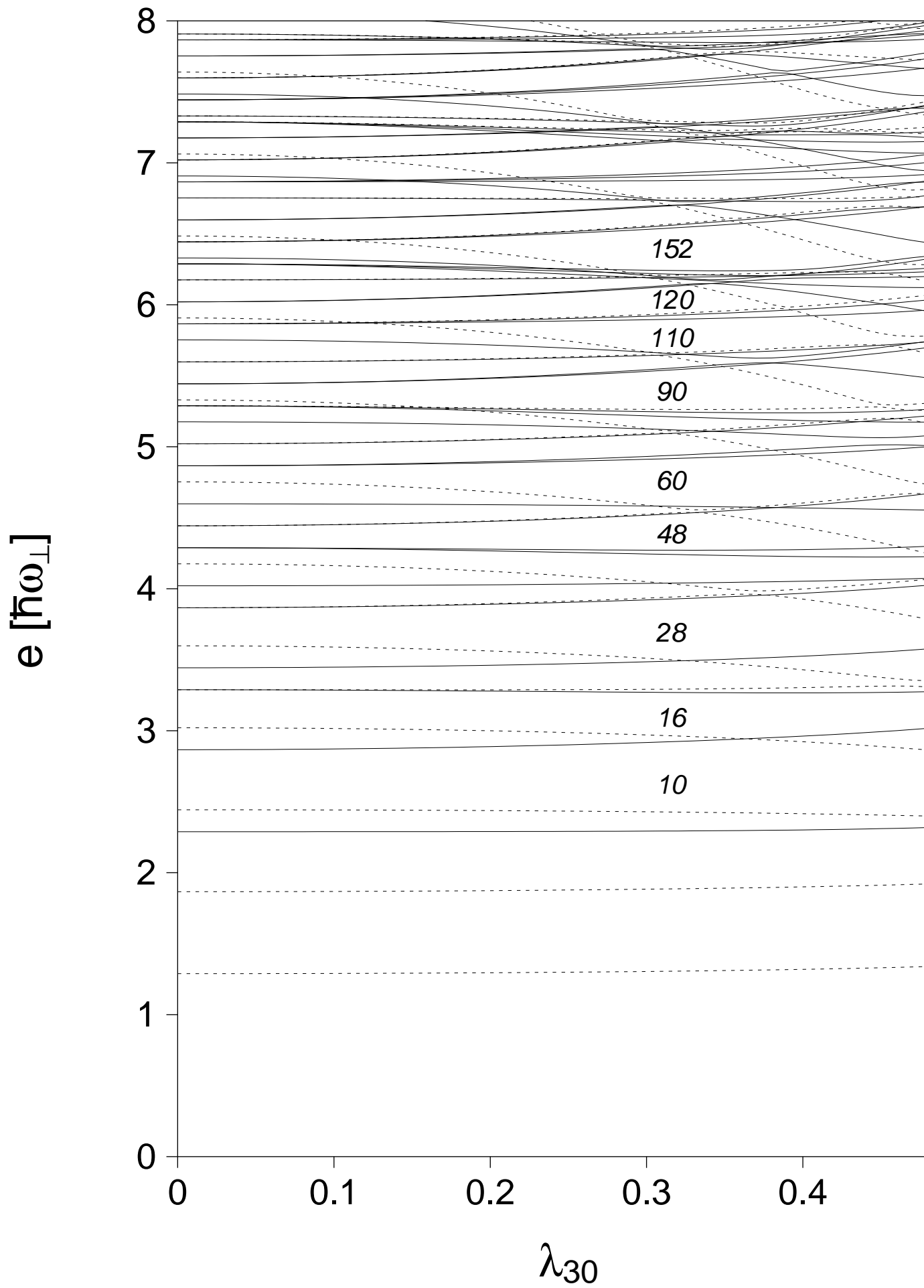
Figure 4: Traces of the monodromy matrices in the neighborhood of the bifurcations of orbits IL (upper panel) and of orbit 3PA (lower panel). The bifurcations occur when $\text{Tr } M = 2$.

Figure 5: Poincaré surfaces of section (ρ, p_{ρ}) defined by $z = 0$ and $p_z < 0$, for $p_{\varphi} = 0$ and $\lambda_{30} = 0.28 \sim 0.31$.

Figure 6: Fourier transforms (9) of the quantum level densities with $E_{\text{max}} = 10\hbar\omega_0$, plotted as functions of s (in unit of $2\pi/\omega_{\perp}$) and λ_{30} .

This figure "fig1-1.png" is available in "png" format from:

<http://arxiv.org/ps/nucl-th/9407004v1>



This figure "fig2-1.png" is available in "png" format from:

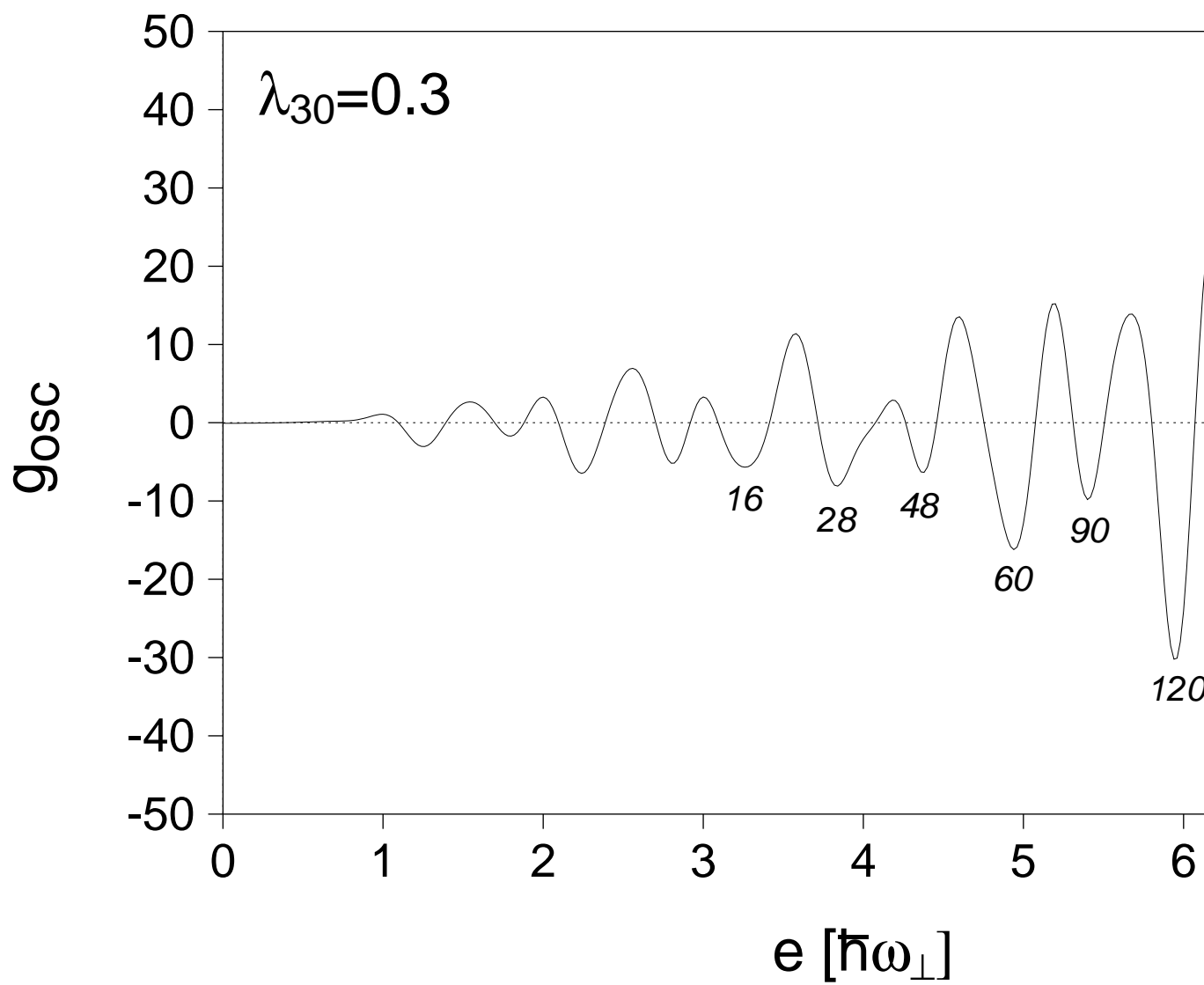
<http://arxiv.org/ps/nucl-th/9407004v1>

This figure "fig1-2.png" is available in "png" format from:

<http://arxiv.org/ps/nucl-th/9407004v1>

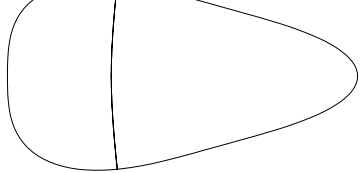
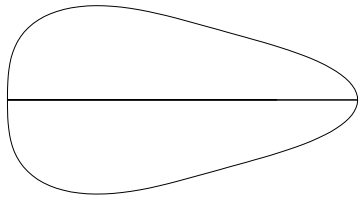
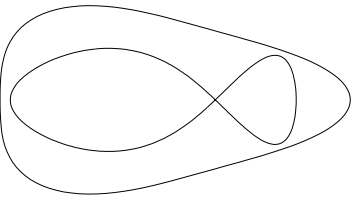
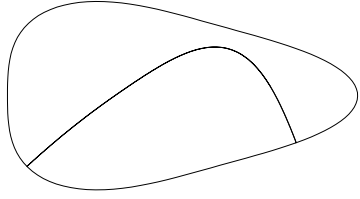
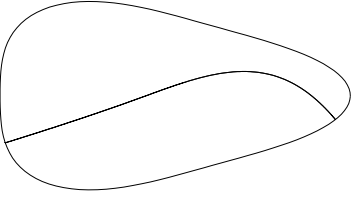
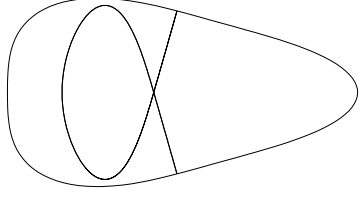
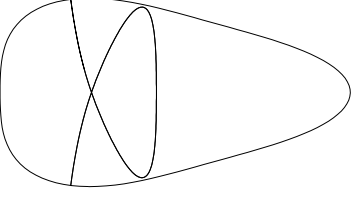
This figure "fig2-2.png" is available in "png" format from:

<http://arxiv.org/ps/nucl-th/9407004v1>



This figure "fig1-3.png" is available in "png" format from:

<http://arxiv.org/ps/nucl-th/9407004v1>

	IA	
	IL	
	PC	
	PE	
		PB
		PD
		PF

This figure "fig1-4.png" is available in "png" format from:

<http://arxiv.org/ps/nucl-th/9407004v1>

